

## Microrheology and structural quantification of hypercoagulable clots: supplement

**LAURA WOLFF-TROMBINI,<sup>1</sup> ADRIEN CERIPA,<sup>2,3</sup> JULIEN MOREAU,<sup>4</sup>  
HUBERT GALINAT,<sup>5</sup> CHLOE JAMES,<sup>1,6</sup> NATHALIE WESTBROOK,<sup>4</sup> AND  
JEAN-MARC ALLAIN<sup>2,3,\*</sup> **

<sup>1</sup> *Université de Bordeaux, UMR1034, Inserm, Biology of Cardiovascular Diseases, Pessac, France*

<sup>2</sup> *LMS, CNRS, Ecole Polytechnique, Institut Polytechnique de Paris, Palaiseau, France*

<sup>3</sup> *Inria, Palaiseau, France*

<sup>4</sup> *Université Paris-Saclay, Institut d'Optique Graduate School, CNRS, Laboratoire Charles Fabry, Palaiseau, France*

<sup>5</sup> *CHU de Brest, Service d'Hématologie Biologique, Brest, France*

<sup>6</sup> *CHU de Bordeaux, Laboratoire d'Hématologie, Pessac, France*

\* [jean-marc.allain@polytechnique.edu](mailto:jean-marc.allain@polytechnique.edu)

---

This supplement published with Optica Publishing Group on 19 July 2023 by The Authors under the terms of the [Creative Commons Attribution 4.0 License](https://creativecommons.org/licenses/by/4.0/) in the format provided by the authors and unedited. Further distribution of this work must maintain attribution to the author(s) and the published article's title, journal citation, and DOI.

Supplement DOI: <https://doi.org/10.6084/m9.figshare.23608416>

Parent Article DOI: <https://doi.org/10.1364/BOE.492669>

# Supporting material

## Microrheology and structural quantification of hypercoagulable clots

LAURA WOLFF-TROMBINI,<sup>1</sup> ADRIEN CERIPA,<sup>2,3</sup> JULIEN MOREAU,<sup>4</sup> HUBERT GALINAT,<sup>5</sup> CHLOE JAMES,<sup>1,6</sup> NATHALIE WESTBROOK,<sup>4</sup> AND JEAN-MARC ALLAIN<sup>2,3,\*</sup>

<sup>1</sup>Université de Bordeaux, UMR1034, Inserm, Biology of Cardiovascular Diseases, Pessac, France

<sup>2</sup>LMS, CNRS, Ecole Polytechnique, Institut Polytechnique de Paris, Palaiseau, France

<sup>3</sup>Inria, Palaiseau, France

<sup>4</sup>Université Paris-Saclay, Institut d'Optique Graduate School, CNRS, Laboratoire Charles Fabry, Palaiseau, France

<sup>5</sup>CHU de Brest, Service d'Hématologie Biologique, Brest, France

<sup>6</sup>CHU de Bordeaux, Laboratoire d'Hématologie, Pessac, France

\*[jean-marc.allain@polytechnique.edu](mailto:jean-marc.allain@polytechnique.edu)

### 1. Determination of the moduli from the Brownian motion

Once the Brownian motion of a bead has been recorded, we follow the procedure described in Schnurr et al. (Ref. 10 of the main article). We recall here the main steps of the procedure:

The optical setup records the normalized voltages associated with the in-plane motion of the bead. Each normalized voltage is transformed into a position through its calibration factor, leading to the in-plane coordinates:  $\mathbf{x}(t)$  and  $\mathbf{y}(t)$ .

#### a. Power spectral density

The first step is to convert these positions into their power spectral densities (PSD)  $\{\mathbf{x}^2\}$  and  $\{\mathbf{y}^2\}$ . This is done through the “periodogram” function in Matlab. Note that the PSD are function of the frequency and not of the time. The PSD is very noisy, due to the measurement noise: figure S1(a) shows a typical PSD before filtering.

We then applied a moving average filter, through the “smooth” function in Matlab. The averaging was done on a window of 32.5 Hz, representing 63 points. As the moving average distorts the signal at its extremities, we didn't apply any filter for frequencies below 2.0 Hz (so on the 4 first points), and we averaged over 2.6 Hz, representing 6 points from 2.0 Hz and 97.5 Hz. Figure S1(b) shows a typical PSD after moving average filtering.

In many, but not all, PSD, an artefactual peak is visible around 80 Hz (see figure S1(a)). It is almost certain that this artefact is not related to some mechanical resonance of the fibrin network, but more to a mechanical noise in our system. To remove the peak, a linear adjustment of the log-log curve of the PSD is done in the range of 500 Hz to 2 kHz. Then, the difference between this linear adjustment and the data is done over a range of 40 Hz to 2 kHz. Any point deviating from more than 0.8 (1.2 the variance of the signal noise on this range) is replaced by the linear fit. A careful visual validation was done after, for each PSD. The figure S1(c) shows the same typical PSD after this filtering.

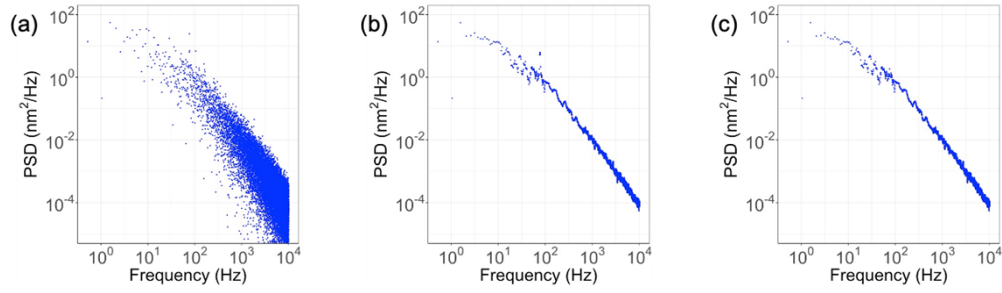


Fig. S1. Power spectral density of a typical clot (in the y-direction): (a) before applying a moving average filtering; (b) after the moving average filtering, with a noise peak at 80 Hz; (c) after all the treatments. The PSD have been truncated at 10 kHz, which is the cutoff frequency of the quadrant photodiode.

## b. Modulus computation for each direction

Once the PSD filtered, we compute the complex moduli of the material, by first computing its complex compliance  $\alpha^*(\omega) = \alpha'(\omega) + i\alpha''(\omega)$ . Indeed, for a bead of radius  $R$ , moving in an incompressible material, and in the small displacement limit, the complex compliance  $\alpha^*(\omega)$  is linked to the complex modulus  $G^*(\omega)$  through:

$$\alpha^*(\omega) = \frac{1}{6\pi R G^*(\omega)}.$$

The imaginary part of the compliance is linked to the PSD of the motion through the fluctuation-dissipation theorem:

$$\{x^2\} = \frac{2k_B T \alpha''(\omega)}{\omega}$$

this implies that

$$\alpha''(\omega) = \frac{\omega \{x^2\}}{2k_B T}.$$

Then, assuming that the compliance is an analytic function (regular), one can use the Kramer-Koning relation to determine the value of the real part of the compliance:

$$\alpha'(\omega) = \frac{2}{\pi} \mathcal{P} \int_0^\infty \frac{\zeta \alpha''(\zeta)}{\zeta^2 - \omega^2} d\zeta$$

The integral is a principal integral, as it is singular at  $\omega$ . To compute this integral, we use the Maclaurin's formula, as suggested by Ohta and Ishida [Ohta1988].

Finally, one has the real (storage) and imaginary (loss) moduli:

$$G'(\omega) = \frac{1}{6\pi R} \frac{\alpha'(\omega)}{\alpha'(\omega)^2 + \alpha''(\omega)^2}$$

$$G''(\omega) = -\frac{1}{6\pi R} \frac{\alpha''(\omega)}{\alpha'(\omega)^2 + \alpha''(\omega)^2}$$

For each bead, we end up with two moduli for the direction x, and two moduli for the direction y. As we didn't observe any systematic asymmetry in the Brownian motion, we average the two of them.

## 2. Cleaning of the skeletonized confocal images

After recovering the structural data (from the skeletonization) with Fiji, we observe extremely short fibers (see Fig. S2). These fibers do not correspond to real fibers, but are due to erroneous branchpoints. They can be created by a thick intersection of multiple fibers, which leads to multiple short branches during skeletonization (in the blue circle of Figure S2). Thick fibers can also lead to very short fibers, almost perpendicular to the main one (in the red circle of Figure S2).

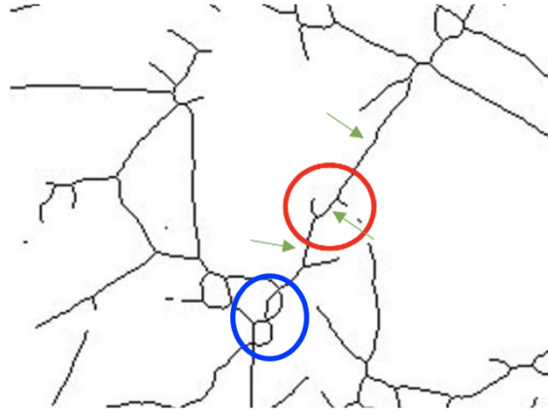


Fig. S2. Micro-fibers and branchpoints creation during skeletonisation. Green arrows show three split fibers, which should be 1 fiber, because of the surrounding microfibers (surrounded in red). Blue circle shows the non-existent branchpoints creating during the intersection of several fibers.

The first case detects more branchpoints than necessary at an intersection, and creates several small non-existent branches. The second case cuts long fibers into several sections, strongly reducing the length of the fiber. It also creates short fibers. Thus, they increase artificially the branching density, the number of fibers, and decrease artificially the fibers length.

To clean the image, our first step is to remove the terminal micro-branches. To do so, we define a cutoff length, which is the typical width of the fluorescence signal of a fiber. We consider that any segment shorter than this length is a spurious branch, and it will be deleted. If the segment is a terminal segment, we delete the segment and the only associated branchpoint. The two remaining segments that were also connected to this branch point are then merged into one larger segment (see Fig. S3, green circle).

The second step is to suppress the artificial branches at the intersection. To do so, we calculate the Euclidean distance between branchpoints. We consider that branchpoints which are closer than twice the cutting length are in fact a single intersection. Thus, we merge them, by creating a single branchpoint at their barycenter. Segments that were connected to the two deleted branchpoints are in turn deleted (see Fig. S3, red circle).

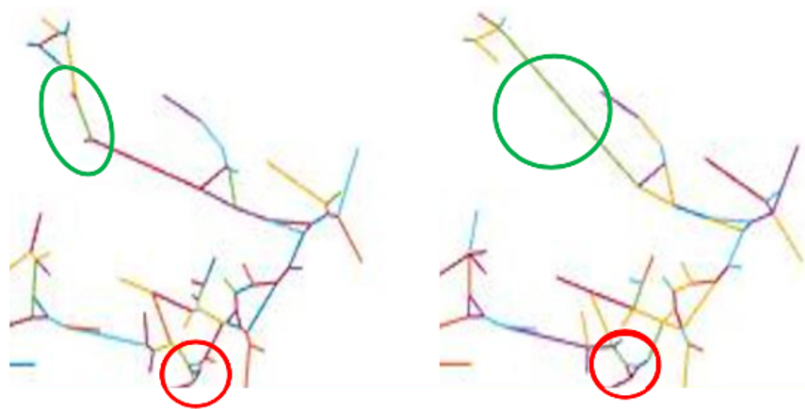


Fig. S3. Skeletonized image before and after corrections. Left: an area of the skeletonized image, prior correction. Right: The same area of the skeleton. The green circle shows a long fiber artificial cut by erroneous micro-branches. The red circle shows the correction of an intersection region.

On a global scale, the skeleton keeps a similar appearance, while on a small scale, as we can see in Figure S3, some artifacts were corrected. This strongly modifies the length distribution. This procedure leaves some artifacts. However, trying to correct too much the image pushes the other way around, with the suppression of short, visible, branches.

### 3. Statistical distributions of the PSD and of the moduli in case of fibrinogen and Factor VIII-enrichment.

Figure S4 shows the distributions of PSD after filtering for the fibrinogen-enrichment experiments, for both the control and the enriched clots. Figure S5 shows the distributions of moduli for the same experiment.

For all graphics, the points represent the 50% quantile of all the controls from the fibrinogen-enriched clots, while the grey zone represents the region between the 25 and 75% quantile (of the same clots). The distribution is obtained by mixing all our data: 3 Brownian motions per beads, 3 to 4 beads per clot and all the clots (6 for the control, 10 for the fibrinogen-enriched).

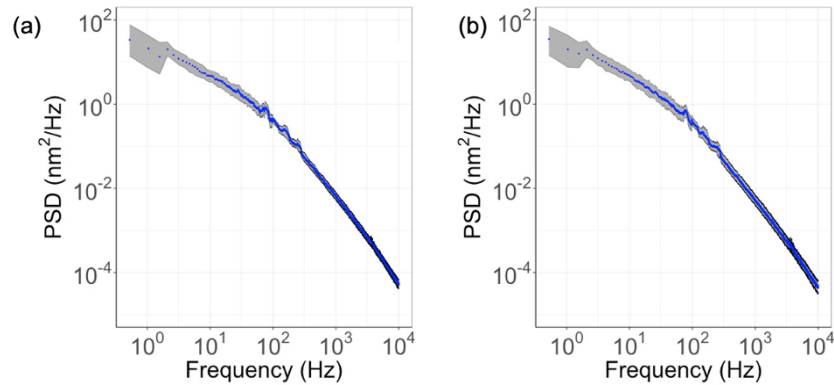


Fig. S4. Distribution of PSD after filtering for the fibrinogen-enrichment experiments: (a) control, and (b) enriched clots. The blue points represent the 50% quantile (the median) of all the recorded Brownian motions for this condition. The grey zone represents the region between the 25 and 75% quantile (of the same clots).

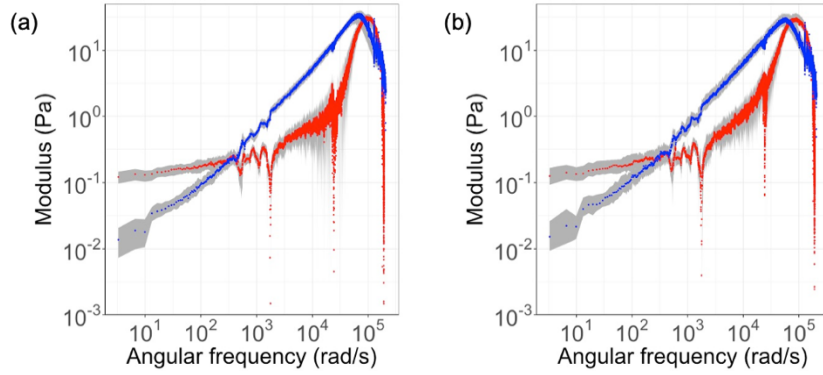


Fig. S5. Distribution of moduli for the fibrinogen-enrichment experiment: (a) control, and (b) enriched clots. The points represent the 50% quantile (the median) of all the recorded Brownian motions for this condition. The grey zone represents the region between the 25 and 75% quantile (of the same clots). The red points are the storage modulus, and the blue points the loss modulus.

Figure S6 shows the distributions of PSD after filtering for the Factor VIII-enrichment experiments, for both the control and the enriched clots. Figure S7 shows the distributions of moduli for the same experiment.

For all graphics, the points represent the 50% quantile of all the controls from the fibrinogen-enriched clots, while the grey zone represents the region between the 25 and 75% quantile (of the same clots). The distribution is obtained by mixing all our data: 3 Brownian motions per beads, 3 to 4 beads per clot and all the clots (6 for the control, 10 for the fibrinogen-enriched).

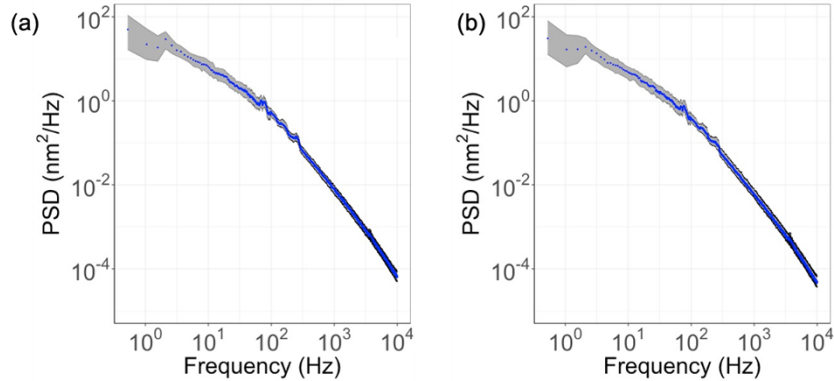


Fig. S6. Distribution of PSD after filtering for the factor VIII-enrichment experiments: (a) control, and (b) enriched clots. The blue points represent the 50% quantile (the median) of all the recorded Brownian motions for this condition. The grey zone represents the region between the 25 and 75% quantile (of the same clots).

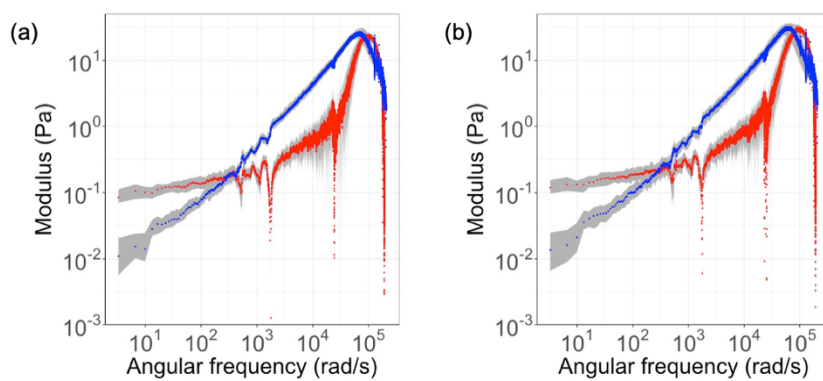


Fig. S7. Distribution of moduli for the Factor VIII-enrichment experiment: (a) control, and (b) enriched clots. The points represent the 50% quantile (the median) of all the recorded Brownian motions for this condition. The grey zone represents the region between the 25 and 75% quantile (of the same clots). The red points are the storage modulus, and the blue points the loss modulus.